scientific reports

Check for updates

OPEN

Comprehensive metabolomics study identifies SN-38 organ specific toxicity in mice

Xiaodong Zhu[1], Ya Huang[2], Jianguo Liu[1], Bo Kong[1], Changmeng Cui[1] & Guangkui Han[1]✉

SN-38 (7-ethyl-10-hydroxycamptothecin), the active metabolite of irinotecan, is a crucial anticancer agent frequently studied in drug delivery systems. Irinotecan (CPT-11) is used to treat various solid tumors but is associated with adverse effects such as nausea, vomiting, diarrhea, and steatohepatitis. However, the precise biochemical pathways underlying these side effects remain unclear. To explore SN-38's toxic mechanisms and provide insights for clinical applications of SN-38 delivery systems, we performed untargeted metabolomics to assess metabolic changes in the lungs, heart, stomach, blood, spleen, intestine, liver, and kidneys of SN-38-exposed male mice. Mice were divided into two groups: SN-38 (20 mg/kg/day intraperitoneal) and control (blank solvent). Gas chromatography-mass spectrometry (GC-MS) identified significant metabolic disturbances in all tissues. Specifically, 24, 15, 12, 21, 35, 26, 18, and 28 differential metabolites were detected in the lungs, heart, stomach, blood, spleen, intestine, liver, and kidneys, respectively. KEGG pathway enrichment revealed significant changes in metabolic pathways across these organs, particularly in purine, pyrimidine, amino acid, and glyceric acid metabolism, implicating disruptions in protein synthesis, cellular homeostasis, energy metabolism, and antioxidant defenses. This study is the first to characterize SN-38's multi-organ toxicity using metabolomics.

Keywords SN-38 (7-ethyl-10-hydroxycamptothecin), Toxicity mechanism, Gas chromatography mass spectrometry, Metabolomics

Ethyl-10-hydroxycamptothecin (SN-38) is a highly potent anticancer agent and the active metabolite of irinotecan (CPT-11), a DNA topoisomerase I inhibitor commonly used in the treatment of various solid tumors, including colorectal, gastric, pancreatic, small cell lung, cervical, and ovarian cancers. Despite its effectiveness, irinotecan is associated with significant adverse effects, such as nausea, vomiting, severe diarrhea, and steatohepatitis[1–3]. SN-38, which is 100 to 1,000 times more cytotoxic than irinotecan, is primarily responsible for the drug's therapeutic activity[4]. However, the clinical application of SN-38 is significantly hindered by its poor solubility and chemical instability, which limit its efficient delivery for cancer treatment. To overcome these limitations and enhance SN-38's therapeutic potential, advanced drug delivery systems, such as nanoparticles, liposomes, and micelles, have been developed. These systems improve the solubility and stability of SN-38, increasing its bioavailability and therapeutic effectiveness. Several of these drug delivery platforms are currently undergoing clinical trials[5].

SN-38 exerts its cytotoxic effects by inhibiting topoisomerase I, leading to DNA damage and the subsequent apoptosis of cancer cells. However, this mechanism is not unique to cancer cells and often results in collateral damage to healthy tissues, posing a significant challenge to its clinical application.

Metabolomics, the comprehensive analysis of small-molecule metabolites in biological systems, has progressed considerably due to advancements in sophisticated analytical techniques and bioinformatics tools. Gas chromatography-mass spectrometry (GC-MS) is particularly advantageous for untargeted metabolomics studies due to its high separation efficiency, reproducibility, and access to extensive metabolite libraries. These features make GC-MS an ideal platform for investigating the complex metabolic changes associated with drug-induced toxicity[6,7].

Although SN-38's neurotoxic potential has been documented through targeted brain metabolomics[8], its broader organ-specific toxicity profile remains unexplored. Here, we employ a multi-organ metabolomics approach to map systemic metabolic disruptions, revealing previously unrecognized hepatic and cardiac vulnerability hotspots.By examining metabolic changes across multiple organs, including the lungs, heart, stomach, serum, spleen, liver, intestine, and kidneys, this research seeks to elucidate the biochemical pathways

[1]Department of Neurosurgery, Affiliated Hospital of Jining Medical University, Jining 272000, China. [2]College of Traditional Chinese Medicine, Shandong Polytechnic College, Jining 272000, China. ✉email: hanguangkui1997@163.com

involved in SN-38 toxicity. The findings are expected to provide a deeper understanding of SN-38's toxicological effects and may help identify potential metabolic biomarkers. Ultimately, this research could contribute to developing strategies for mitigating irinotecan-induced toxicity and offer experimental support for the clinical translation of SN-38-based delivery systems.

Methods

Chemicals and reagents

SN-38 was purchased from MedChemExpress (Shanghai, China). Dimethyl sulfoxide (DMSO) was obtained from Tianjin Yongda Chemical Reagent Co., Ltd. (Tianjin, China). Heptadecanoic acid (purity 98%), methanol (chromatographic grade), and pyridine were sourced from Macklin Biochemical Co., Ltd. (Shanghai, China). O-Methylhydroxylamine hydrochloride (purity 98%) was purchased from J&K Scientific Ltd. (Beijing, China). N, O-bis(trimethylsilyl)trifluoroacetamide (containing 1% trimethylchlorosilane) was obtained from Sigma-Aldrich (St. Louis, MO, USA). Purified water was provided by Hangzhou Wahaha Group Co., Ltd. (Hangzhou, China).

Animal treatment

In this study, the resource equation method was employed to determine the appropriate sample size. A total of 20 six-week-old male Kunming mice were purchased from Jinan Pengyue Experimental Animal Breeding Co., Ltd. (Jinan, China). The use of male mice helps minimize hormone-related variability, eliminating confounding factors such as the estrous cycle[9]. These mice were housed under controlled conditions at a stable temperature of 22 ± 2 °C, with humidity maintained between 60 and 70%, and a 12-hour light/dark cycle. Standard food and water were provided ad libitum throughout the study. A one-week acclimatization period was observed prior to the commencement of the main experiment. The mice were then randomly divided into control and test groups, with 10 mice in each group. For the experimental procedure, SN-38 was dissolved in a solution of sodium chloride and 5% DMSO to the desired concentration. The test group ($n = 10$) received an intraperitoneal injection of SN-38 (20 mg/kg) daily for one week. The drug administration schedule was based on existing studies[10]. The control group ($n = 10$) received an equal volume of the blank solvent mixture (DMSO and saline, 1:9 ratio). This study has been reported in accordance with the ARRIVE guidelines. This study was conducted in accordance with the "Guidelines for Ethical Review of Animal Welfare" (GB/T 35892–2018) and was approved by the Ethics Committee of the Affiliated Hospital of Jining Medical University (Approval No.: JNMC-2022-DW-041).

Sample collection and preparation

Two weeks later, the mice from both groups were euthanized by administering an overdose of sodium pentobarbital (80 mg/kg). Blood samples (1 mL) were taken through enucleation, and serum was separated by centrifugation at 4 °C at 4000 rpm for 10 min. The serum was immediately mixed with cold methanol (1:3 v/v) to inhibit enzymatic activity and stored at −80 °C.To prevent ongoing metabolic processes immediately after euthanasia, tissues (lung, heart, stomach, spleen, liver, intestine, kidney) were snap-frozen in liquid nitrogen within 30 s and stored at −80 °C.

To prepare the serum samples, 100 µL of serum was combined with 350 µL of heptanoic acid (10 µg/mL, used as an internal standard) dissolved in methanol. Procedural blanks (methanol without biological material) were processed in parallel with each extraction batch. The mixture was then centrifuged at 14,000 rpm for 15 min at 4 °C. The resulting supernatant was evaporated under nitrogen gas at 37 °C. The dried residue was incubated with 80 µL of O-methylhydroxylamine hydrochloride dissolved in pyridine at 70 °C for 2 h. Subsequently, 100 µL of N, O-bis(trimethylsilyl)trifluoroacetamide (with 1% trimethylchlorosilane) was added, and the mixture was incubated again at 70 °C for 1 h. After a brief centrifugation at 14,000 rpm for 2 min at 4 °C, the solution was filtered through a 0.22 µm membrane and prepared for GC-MS analysis.

For tissue sample preparation, 50 mg of each tissue was homogenized in methanol. The homogenate was then combined with 50 µL of heptanoic acid (10 µg/mL, internal standard) dissolved in methanol and centrifuged at 14,000 rpm for 15 min at 4 °C. The supernatant was incubated with 80 µL of O-methylhydroxylamine hydrochloride dissolved in pyridine at 70 °C for 90 min. This was followed by an additional incubation with N, O-bis(trimethylsilyl)trifluoroacetamide containing 1% trimethylchlorosilane for 60 min at the same temperature. After incubation, the samples were filtered through a 0.22 µm membrane. Quality control (QC) samples were prepared by mixing 10 µL of each sample from the control and SN-38 group, thoroughly mixed, and aliquoted into individual vials. To reduce the degradation of volatile derivatives, QC samples were sealed with nitrogen and stored at −80 °C. QC aliquots were injected every 10 experimental samples throughout the analytical sequence to monitor instrumental stability. The relative standard deviation (RSD) of QC samples should be less than 30%.

Pathological examination

Tissues from the lung, heart, stomach, spleen, intestine, liver, and kidney were collected and immersed in 4% paraformaldehyde for overnight fixation. After fixation, samples were dehydrated through a graded ethanol series (70% and 95% ethanol, 1 h each) and embedded in paraffin blocks. Sections of 4 µm thickness were prepared using a microtome (Leica, Germany). For deparaffinization, slides were cleared in xylene (three changes, 5 min each) and gradually hydrated through a graded ethanol series (100%, 96%, 80%, 70%, and 50%, 2 min per step). Hematoxylin and eosin (H&E, Sigma-Aldrich, USA) staining was performed to assess histopathological alterations. Whole-slide imaging was conducted using a PANNORAMIC MIDI slide scanner (3DHISTECH, Hungary), and digital sections were analyzed with Case Viewer 2.4 software (3DHISTECH, Hungary) to evaluate morphological changes across all organs.

GC-MS-based metabolomics

Metabolomics analysis was carried out using a 7000 C mass spectrometer connected to a 7890B gas chromatography system, featuring an HP-5MS fused silica capillary column (Agilent Technologies, USA). Prior to sample analysis, system suitability was verified by injecting methyl stearate (10 ppm in heptane) five times. The acceptance criteria required retention time RSD < 0.1 min, peak area RSD < 5%, and signal-to-noise ratio > 50:1. Samples were injected at a split ratio of 50:1, and helium served as the carrier gas with a flow rate of 1 mL/min. The injection port, transfer line, and ion source temperatures were set to 280 °C, 250 °C, and 230 °C, respectively. Electron impact ionization was employed at −70 eV, with a spectral acquisition rate of 20 spectra per second. The mass spectrometry analysis used electron spray ionization, scanning a mass-to-charge ratio (m/z) range from 50 to 800.

Data processing and analysis

Raw data were processed using Mass Hunter software (v.B.07.00; Agilent Technologies) with predefined parameters (peak width: 0.1 min, signal-to-noise threshold ≥ 3:1). Data matrix filtering removed features with > 20% missing values across samples. Missing values were imputed using 50% of the minimum positive value for each metabolite. Background signals from procedural and solvent blanks were subtracted. The metabolites identified in this study were classified as Level 2, representing putatively annotated compounds[11].Metabolites were initially identified through the NIST 14 GC-MS library (similarity score > 80%) and validated against a custom library ("New Library") constructed from quality control (QC) samples. All identifications underwent dual-blind manual verification. Putative annotations required spectral similarity > 80% and retention time consistency (deviation < 2%). Metabolites showing > 30% relative standard deviation (RSD) across QC replicates were excluded. Batch effects were mitigated via randomized sample sequences and QC-based LOESS normalization (MetaboAnalyst 6.0)[12].

Multivariate analyses (PCA/OPLS-DA) were performed in SIMCA-P 14.0 after peak area normalization. Model robustness was evaluated through 200 permutation tests ($p < 0.05$). Differentially expressed metabolites were selected using variable importance in projection (VIP) > 1.0 and $p < 0.05$ (two-tailed Student's t-test with Benjamini-Hochberg correction). Downstream analyses included hierarchical clustering (heatmaps) and KEGG pathway enrichment (MetaboAnalyst 6.0)[13–16].

Statistical analysis

IBM SPSS Statistics 19 was used for normality (Shapiro-Wilk test) and homogeneity (Levene's test) assessments. Only metabolites passing normality ($p > 0.05$) and homogeneity ($p > 0.05$) criteria were included in parametric statistical tests.

Results

GC-MS tics

As illustrated in Fig. 1, the total ion chromatograms (TICs) of quality control (QC) samples demonstrate chromatographic stability across analytical batches, characterized by consistent retention time (RT) alignment and stable peak intensity profiles. The overlapping traces reflect sustained instrument performance during continuous analysis, with high peak capacity and baseline resolution throughout the analytical run.

Multivariate analysis of metabolomics data

Unsupervised PCA demonstrated tissue-specific metabolic divergence between SN-38-treated and control groups across seven organs (cumulative R2X: 0.28–0.59), with maximal separation in hepatic (R2X = 0.519) and pulmonary (R2X = 0.589) tissues (Table 1). Supervised OPLS-DA exhibited strong discriminative performance, showing near-complete variance explanation in cardiac (R2Y = 0.999) and splenic (R2Y = 1.000) models (Q2:

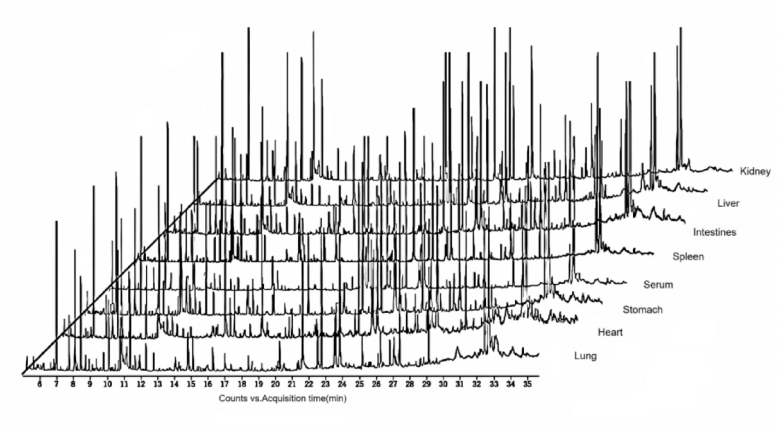

Fig. 1. Representative gas chromatography–mass spectrometry (GC–MS) total ion chromatograms (TICs) from the quality control (QC) samples.

Tissues	Model type	R2X(cum)	R2Y(cum)	Q2(cum)
Lung	PCA	0.589	/	0.413
	OPLS-DA	0.578	0.994	0.885
Heart	PCA	0.296	/	−0.0822
	OPLS-DA	0.298	0.999	0.86
Stomach	PCA	0.368	/	0.074
	OPLS-DA	0.28	0.964	0.747
Serum	PCA	0.327	/	0.0754
	OPLS-DA	0.346	0.998	0.896
Spleen	PCA	0.436	/	0.215
	OPLS-DA	0.507	1	0.88
Intestines	PCA	0.485	/	0.161
	OPLS-DA	0.424	0.984	0.788
Liver	PCA	0.519	/	0.328
	OPLS-DA	0.468	0.983	0.908
Kidney	PCA	0.41	/	0.179
	OPLS-DA	0.328	0.984	0.86

Table 1. PCA and OPLS-DA parameter scores.

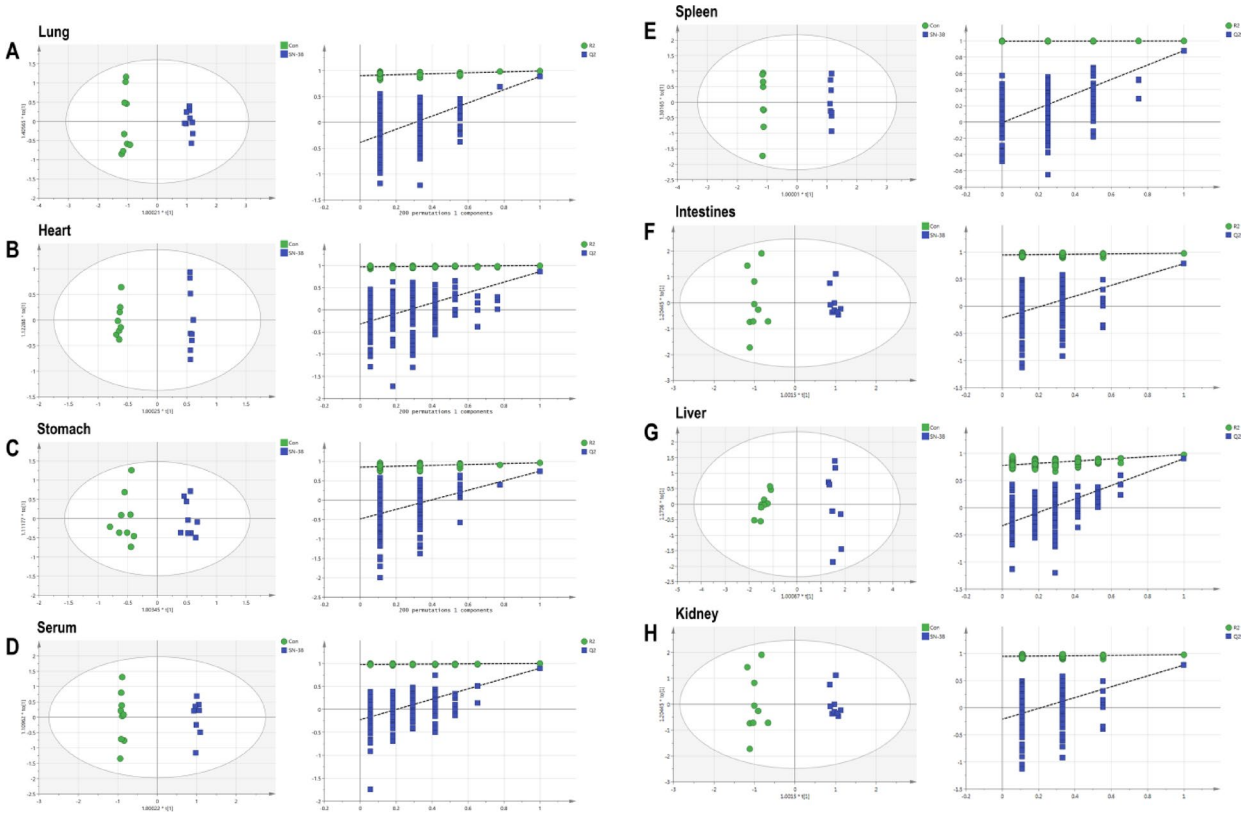

Fig. 2. OPLS-DA score plots and results from permutation tests.

0.75–0.91; Table 1). Permutation testing ($n = 200$) confirmed model validity (all permuted Q2 intercepts < 0; $p < 0.05$)(Fig. 2), though caution is advised when interpreting cardiac/splenic signatures due to potential overfitting risks inherent to high-dimensional omics models[17].

Identification of metabolic changes in samples

Metabolite identification was conducted using a well-established mass spectrometry database, beginning with spectral comparisons from the Agilent Fiehn GC/MS Metabolomics RTL Library. The criteria for identifying metabolites included the variable importance in projection (VIP) score and p-value, with a VIP score above

1 and a p-value below 0.05 considered significant indicators of potential metabolites. Additionally, a fold-change greater than 1 signified an upward trend in metabolite levels, while a fold-change less than 1 indicated a downward trend. Table 2 summarizes the metabolic alterations observed across different tissues in the study groups, and the comparison of the distribution of biomarkers in each tissue are shown in Fig. 3.In total, 69 metabolites were identified as significantly altered in serum and tissues following SN-38 treatment.

In lung tissue, 24 metabolites exhibited a downregulated trend, including amino acids, lactate, fatty acids, and others. In the heart, 15 metabolites were identified, with 4 showing upregulation (adenine, creatinine, adenosine) and 11 showing downregulation. In the stomach, SN-38 treatment led to alterations in 12 metabolites, with 8 upregulated (including alanine, valine, proline, serine, aspartic acid, glutamic acid, and threonine) and 4 downregulated (such as ethanolamine and lactate). In the liver, 12 metabolites were upregulated, including palmitic acid, arachidonic acid, stearic acid, cholesterol, and uracil, while 6 metabolites, such as amino acids and galactose, were downregulated. Additionally, 21, 35, 26, and 18 metabolites were downregulated in the serum, spleen, intestine, and kidney, respectively. Clustering analysis of the differential metabolites between the SN-38 and control groups further supported these findings (Fig. 4).

Metabolic pathway analysis

To further evaluate the metabolic changes between the SN-38 and control groups, MetaboAnalyst 6.0 (http://www.metaboanalyst.ca) and the KEGG database (http://www.kegg.jp) were employed to identify the metabolic pathways impacted by SN-38 treatment. Pathways with a raw p-value of less than 0.05 and an impact value greater than 0 were considered potentially disrupted (see Table 3; Fig. 5). The analysis revealed that SN-38 exposure significantly affected several metabolic pathways, including those related to various amino acids, glutathione, purine, pyrimidine, pyruvate, glyoxylate and dicarboxylate metabolism, as well as glycerolipid, glycerophospholipid, and sphingolipid metabolism. The detailed pathway analysis results are presented in Table 3, with a summary in Fig. 5, and a comprehensive metabolic network map in Fig. 7.

Pathological examination

Microscopic examination revealed preserved tissue architecture across all organs: alveolar integrity in the lung, orderly myocardial fiber alignment in the heart, intact gastric mucosa, normal splenic pulp distribution, unaltered intestinal villi, regular hepatic trabeculae, and structurally sound renal glomeruli and tubules. Quantitative assessment of characteristic regions demonstrated no significant histopathological differences between SN-38-treated and control groups ($p > 0.05$), indicating no overt organ damage (Fig. 6).

Discussion

Clinical evidence highlights that the toxicity of irinotecan and its active metabolite, SN-38, predominantly impacts the gastrointestinal tract—manifesting as nausea, vomiting, severe diarrhea, and mucositis—as well as the liver, particularly in the form of steatohepatitis. However, there are also reports of drug-induced toxicity in other organs, including pulmonary fibrosis and lung inflammation[18,19], as well as sinus bradycardia in patients with small round cell carcinoma[20]. In this study, we employed multivariate statistical analysis to assess the effects of SN-38 on major organs and tissues in mice. The novelty of this research lies in its investigation of SN-38's pharmacological mechanisms from a metabolomics perspective, offering a comprehensive evaluation of the metabolic disruptions triggered by SN-38 exposure in mice using GC-MS analysis. Our findings demonstrate that SN-38 induces significant metabolic disturbances in the blood and various tissues. Specifically, 24 metabolites were identified in the lungs, 15 in the heart, 12 in the stomach, 21 in the blood, 35 in the spleen, 26 in the intestine, 18 in the liver, and 28 in the kidney. KEGG pathway enrichment analysis revealed statistically significant alterations in 5 metabolic pathways in the lungs, 8 in the heart, 5 in the stomach, 10 in the blood, 10 in the spleen, 5 in the intestine, 1 in the liver, and 9 in the kidney. To elucidate the distinct pharmacological mechanisms resulting from these varied metabolic changes across different organs, the following sections provide a detailed discussion of these findings. (Fig. 7)

The reduction in ethanolamine and phosphoethanolamine levels suggests a disruption in phospholipid metabolism, which is essential for maintaining the integrity of cell membranes. Glycerol, a crucial component in triglyceride synthesis, also plays a pivotal role in the formation of phospholipids, the primary lipid constituents of pulmonary surfactants. Disruptions in glycerol metabolism may impair the production of phosphatidylcholine, which could result in diminished surfactant synthesis and functionality. This decrease could increase alveolar surface tension, potentially leading to alveolar collapse and reduced lung compliance[21]. The depletion of these metabolites in the lungs may compromise cell membrane stability, making lung tissues more vulnerable to injury.

Furthermore, the observed decrease in taurine levels suggests a weakened antioxidant defense in lung tissue, potentially leading to elevated oxidative stress and subsequent lung damage[22]. Inositol, a critical nutrient known for promoting cell survival and proliferation, is widely used in the treatment of conditions such as respiratory distress syndrome (RDS) and Alzheimer's disease[23]. Additionally, proline and hydroxyproline, key components of collagen, play vital roles in lung tissue repair. The reduction in hydroxyproline levels indicates a hindered repair process, which could further aggravate lung injury[24].

Adenosine plays a crucial role in regulating coronary blood flow and protecting the heart from ischemic damage. Its accumulation is directly implicated in the pathophysiology of atrial fibrillation and neurocardiogenic syncope. Additionally, adenosine is fundamental in the adaptive responses to pulmonary hypertension and heart failure, with its primary effects including the reduction of heart rate, coronary vasodilation, and lowering of blood pressure[25]. Under stress conditions, adenosine levels rise, acting as both a signaling molecule and a cardioprotective agent, indicating a compensatory response to SN-38-induced cardiotoxicity[26]. In this study, the observed increase in the adenosine breakdown product, inosine, supports the hypothesis of enhanced purine

metabolism. The concurrent elevation of adenine and inosine suggests an imbalance in purine metabolism, which may lead to altered nucleotide synthesis and increased oxidative stress, exacerbating cardiac injury.

A disruption in glutathione metabolism is a significant contributor to the pathogenesis of myocardial injury. The reduction of key metabolites, such as glutamate and glycine, causes dysregulation in glutathione metabolism, contributing to various cardiac issues, including myocardial injury, ferroptosis, metabolic disturbances, impaired cardiac function, and cardiac remodeling[27,28]. Previous research has shown that irinotecan significantly impacts oxidative stress parameters in cardiac tissue, with increased lipid peroxidation (elevated TBARS levels), reduced activity of antioxidant enzymes (SOD, CAT, GPx), and decreased glutathione (GSH) levels[29]. These findings underscore the critical role of SN-38-induced oxidative stress in the development of cardiotoxicity.

Proline is vital for protein synthesis and cell growth, as well as for osmoregulation, protein stability, cellular bioenergetics, and antimicrobial or antifungal activity[30]. Elevated levels of proline may indicate an attempt by the stomach to repair damage caused by SN-38. However, if these repair processes become dysregulated, chronic upregulation of such pathways might lead to pathological changes[31]. Abnormal levels of L-alanine and L-glutamate suggest disruptions in amino acid metabolism, which plays a crucial role in energy production and neurotransmitter synthesis. These disruptions could exacerbate oxidative stress, further damaging the gastric mucosa[32]. Glutamate stimulates gastric acid secretion, and chronic or excessive glutamate levels may result in hyperacidity, causing gastric mucosal damage and potentially leading to gastric ulcers. Previous studies have shown that NMDA receptor agonists, which interact with glutamate receptors, increase the incidence of gastric ulcers. Excessive glutamate release or receptor dysfunction may also contribute to gastrointestinal disturbances, such as diarrhea or constipation[33].

Glycine is recognized as a key protective factor against gastrointestinal diseases, particularly in the context of chemically induced colitis and inflammatory bowel disease (IBD). Research suggests that glycine may have protective effects against irinotecan-induced mucositis. Elevated glycine levels in patients with active IBD further highlight its role in alleviating colitis and reducing intestinal inflammation[34]. However, the observed decline in glycine levels in the intestines following SN-38 treatment could worsen intestinal inflammation, emphasizing the need for glycine regulation in managing inflammation. Aspartate is associated with chronic visceral pain and hypersensitivity in patients with colonic inflammation. The RGD (arginine-glycine-aspartate) peptide motif exhibits anti-inflammatory properties in the intestine, helping to maintain gut barrier integrity by upregulating genes such as trefoil factor-3 and mucin[30]. Consequently, aspartate may serve as a biomarker for the severity of inflammatory bowel disease. Additionally, stearic acid has been shown to reduce inflammation caused by bile duct ligation (BDL) by inhibiting inflammatory cell recruitment and NF-κB activation. Previous studies have confirmed that stearic acid may function as a protective metabolite against irinotecan-induced colitis[34].

The elevation of palmitic acid, arachidonic acid, stearic acid, and docosahexaenoic acid (DHA) in the liver of the SN-38 treatment group suggests significant disruptions in lipid metabolism. Arachidonic acid, in particular, is a ω−6 polyunsaturated fatty acid that is abundant in cell membrane phospholipids and lipid droplets. Its activation of macrophages, specifically Kupffer cells, triggers the release of pro-inflammatory cytokines, such as tumor necrosis factor-α (TNF-α) and interleukin-6 (IL-6)[35]. Metabolites of arachidonic acid, produced through the lipoxygenase (LOX) and cyclooxygenase (COX) pathways, including prostaglandins PGE2 and PGD2, further exert pro-inflammatory effects[36]. Additionally, the COX pathway influences the peroxisome proliferator-activated receptor gamma (PPARγ), which is implicated in the development of non-alcoholic fatty liver disease (NAFLD). PPARγ is closely associated with insulin resistance and hepatic steatosis, contributing to the pathogenesis of NAFLD[37].

Palmitic acid, the most prevalent saturated fatty acid, is strongly linked to the development of fatty liver disease. Elevated palmitic acid levels can lead to excessive fat accumulation within hepatocytes, thereby promoting fatty liver formation[38]. Pyrimidine nucleotides, which are essential for DNA synthesis, also play a critical role in cellular signaling and energy metabolism, maintaining cellular homeostasis. Alterations in pyrimidine metabolites, such as thymidine, uracil, and deoxycytidine, have been closely associated with disruptions in pyrimidine metabolism. Studies suggest that such disruptions may contribute to liver damage, resulting in significant hepatocellular dysfunction, including increased oxidative stress, impaired bile acid synthesis, and dysregulation of the glutathione (GSH) biosynthesis pathway[39].

Serine is a crucial source of N5,N10-methylene tetrahydrofolate (MTHF), and its deficiency can lead to MTHF depletion, impairing DNA synthesis and cell division. Additionally, serine acts as an intermediate in the tricarboxylic acid (TCA) cycle, playing a vital role in energy metabolism. A deficiency in serine can result in energy metabolism disorders, thereby disrupting cellular functions[40]. L-serine also reduces the secretion of pro-inflammatory cytokines, including IL-1, IL-17, interferon-γ, and TNF-α, while inhibiting neutrophil-mediated inflammation in macrophages[41]. The downregulation of serine suggests impaired respiratory function[42], and as a key amino acid involved in protein and phospholipid synthesis, its deficiency may further compromise lung tissue repair processes.

A reduction in serum taurine levels may exacerbate systemic oxidative stress and inflammatory responses, which are common in chemotherapy-induced systemic toxicity. Taurine is known for its anti-inflammatory properties, as it inhibits the production of various inflammatory mediators and plays a protective role in intestinal mucosal cells, helping to mitigate damage caused by inflammation and oxidative stress. Studies indicate that decreased serum taurine levels may amplify inflammatory responses, potentially worsening the symptoms and tissue damage associated with inflammatory bowel disease (IBD)[43].

Notably, while SN-38 administration induced marked metabolic disturbances across all eight organs examined, subsequent histopathological evaluation demonstrated no gross morphological alterations in these tissues. This divergence implies that SN-38 toxicity primarily manifests as subcellular or molecular pathway dysregulation, rather than immediate structural compromise. Specifically, the observed metabolomic shifts may represent early adaptive metabolic reprogramming or compensatory biochemical adjustments to cellular stress

Metabolite	HMDB ID	Lung			Heart			Stomach			Serum			Spleen			Intestine			Liver			Kidney		
		VIP	*p*-value	Trend	VIP	*p*-value	Trend	VIP	*p*-value	Trend	VIP	*p*-value	Trend	VIP	*p*-value	Trend	VIP	*p*-value	Trend	VIP	*p*-value	Trend	VIP	*p*-value	Trend
L-Alanine	HMDB0000161	1.43185	0	↓	1.5608	0.003	↓	1.15808	0.023	↑				1.68741	0	↓	1.66198	0.002	↓				1.27615	0	↓
Ethanolamine	HMDB0000149	1.42849	0	↓	1.26673	0	↓	1.4888	0.007	↓	1.33237	0.003	↓	1.18623	0	↓									
Glycine	HMDB0000123				1.40574	0	↓				2.03319	0	↓	1.62385	0	↓	1.41217	0.002	↓				1.3884	0	↓
Uracil	HMDB0000300	1.25803	0	↓	1.52355	0.001	↓							1.1417	0	↓	1.4811	0	↓	1.43853	0.001	↑			
Serine	HMDB0062263	1.00729	0	↓	1.32922	0	↓	1.80309	0.001	↑	1.39477	0	↓	1.44171	0	↓	1.48091	0.005	↓						
L-Threonine	HMDB0000167	1.16436	0	↓				1.28401	0.022	↑	1.6348	0	↓	1.51569	0	↓	1.49606	0.004	↓						
L-5-Oxoproline	HMDB0000267	1.21667	0	↓	1.6697	0	↑							1.44595	0	↓	1.36197	0.008	↓				1.24731	0	↓
L-Aspartic acid	HMDB0000191	1.59829	0	↓				2.03692	0.001	↑				1.667	0	↓	1.1527	0.012	↓						
L-Hydroxyproline	HMDB0000725	1.42872	0	↓																					
Taurine	HMDB0000251	1.64232	0	↓							1.54467	0.043	↓	1.56647	0.001	↓									
Erythritol	HMDB0002994	1.06689	0.001	↓																					
Myristic acid	HMDB0000806	1.12475	0	↓										1.29796	0	↓	1.01626	0.002	↓				1.2056	0.002	↓
Myo-Inositol	HMDB0000211	1.04457	0	↓																1.03526	0.001	↑			
Lactic Acid	HMDB0000190	1.50075	0	↓				2.48085	0	↓	1.28865	0.027	↓	1.82329	0	↓	1.49016	0.009	↓				1.81304	0	↓
Glyceric acid	HMDB0000139	1.25863	0	↓																			1.06429	0.012	↓
Malic acid	HMDB0000744	2.02242	0	↓	2.29639	0	↓				1.99384	0	↓	1.65963	0	↓	1.6327	0.001	↓				1.58496	0.001	↓
Phosphorylethanolamine	HMDB0000224	2.03988	0	↓	1.20574	0.004	↓							2.13797	0.001	↓	2.0118	0	↓				2.50558	0	↓
L-Lysine	HMDB0000182	1.5953	0	↓							1.22089	0.016	↓	1.84087	0	↓	1.59551	0.024	↓	1.0835	0	↓	1.81673	0	↓
L-Tyrosine	HMDB0000158	1.12706	0	↓							2.05449	0	↓	1.58114	0	↓	1.52078	0.004	↓	1.12152	0	↓	1.06791	0.004	↓
11-Octadecenoic acid	HMDB0003231	1.19638	0	↓																					
Arachidic acid	HMDB0002212	1.0138	0	↓													1.01931	0.002	↓				1.0305	0.047	↓
MG(0:0/18:1(9Z)/0:0)	HMDB0011537	1.15517	0.04	↓																					
MG(0:0/18:0/0:0)	HMDB0011535	1.13729	0	↓																			1.43048	0	↓
L-Valine	HMDB0000883							1.55952	0.004	↑	1.07133	0.034	↓	1.59536	0	↓	1.69261	0.002	↓						
L-Proline	HMDB0000162							2.03295	0	↑	1.25163	0.001	↓	1.69751	0	↓									
Pipecolic acid	HMDB0000070							1.63311	0.002	↑															
L-Glutamic acid	HMDB0000148				1.63346	0.004	↓	1.44133	0.009	↑	1.69197	0	↓	1.52771	0	↓				1.00108	0.003	↓	1.12096	0.003	↓
Petroselinic acid	HMDB0002080							1.15756	0.023	↓							1.4087	0	↓	1.15674	0.006	↑			
Succinic acid	HMDB0000254							2.12961	0.001	↓	1.81357	0.001	↓										2.12777	0	↓
Phenylalanine	HMDB0000159													1.38987	0.001	↓	1.55429	0.005	↓				1.08807	0.002	↓
L-Isoleucine	HMDB0000172													1.53587	0	↓	1.74659	0.002	↓				1.11152	0.001	↓
L-Methionine	HMDB0000696				1.70484	0	↓				1.3893	0.001	↓	1.45341	0	↓	1.59407	0.004	↓						
L-Ornithine	HMDB0000214										1.56836	0.004	↓										1.56418	0	↓
L-Tryptophan	HMDB0000929										1.55396	0.001	↓	2.11505	0.001	↓									
Cholesterol	HMDB0000067										1.4858	0.004	↓				1.2265	0	↓	1.27767	0.001	↑			
5-Aminovaleric acid	HMDB0003355										1.67392	0.009	↓												
Dodecanoic acid	HMDB0000638													1.12705	0.043	↓									
Stearic acid	HMDB0000827													1.18693	0.001	↓	1.25653	0	↓	1.23325	0.001	↑			
Urea	HMDB0000294													1.44196	0.001	↓									
L-Arabitol	HMDB0001851													1.43152	0.005	↓							1.28594	0.006	↓
L-Leucine	HMDB0000687													1.53919	0	↓	1.67731	0.003	↓				1.02754	0.003	↓

Continued

Metabolite	HMDB ID	Lung			Heart			Stomach			Serum			Spleen			Intestine			Liver			Kidney		
		VIP	*p*-value	Trend	VIP	*p*-value	Trend	VIP	*p*-value	Trend	VIP	*p*-value	Trend	VIP	*p*-value	Trend	VIP	*p*-value	Trend	VIP	*p*-value	Trend	VIP	*p*-value	Trend
D-Mannitol	HMDB0000765																			1.13177	0.001	↑	1.25664	0.001	↓
Asparagine	HMDB0000168													1.94572	0	↓							1.4482	0.002	↓
D-Glucose	HMDB0000122										2.3219	0	↓												
Gluconic acid	HMDB0000625																			1.05046	0.004	↓			
Oxalic acid	HMDB0002329																			1.21659	0.001	↑			
Ribitol	HMDB0000508																			1.0579	0.009	↓			
Hexadecane	HMDB0033792																			1.58377	0	↑			
Docosahexaenoic acid	HMDB0002183													1.41852	0.006	↓	1.01199	0.004	↓	1.32795	0.001	↑	1.33549	0.001	↓
2-Aminooctanoic acid	HMDB0000991																						1.89931	0	↓
D-Arabitol	HMDB0000568																						1.2075	0.003	↓
2-Phenylbutyric acid	HMDB00329																						1.12875	0.012	↓
Glycerol	HMDB0000131	1.30896	0	↓							1.1409	0.001	↓	1.30749	0	↓	1.08352	0	↓				1.46021	0	↓
Niacinamide	HMDB0001406	1.00698	0	↓																					
Hypoxanthine	HMDB0000157				1.17903	0.005	↓																		
Adenine	HMDB0000034				1.15503	0.033	↑																		
MG(16:0/0:0/0:0)	HMDB0011564				1.01955	0.005	↓																1.49898	0	↓
Inosine	HMDB0000195				1.32579	0.002	↑																		
Adenosine	HMDB0000050				1.91973	0.001	↑																		
Citric acid	HMDB0000094										1.64524	0.001	↓												
Beta-Alanine	HMDB0000056													1.6621	0	↓									
4-Hydroxybenzyl alcohol	HMDB0011724													1.26064	0.003	↓									
Palmitic acid	HMDB0000220													1.19475	0.001	↓				1.0434	0	↑			
Ribothymidine	HMDB0000884													1.2569	0.003	↓									
Uridine	HMDB0000296													1.32668	0.005	↓									
N-Dodecane	HMDB0031444																1.22568	0.038	↓	1.42558	0.001	↑			
Arachidonic acid	HMDB0001043																1.12277	0.005	↓	1.55127	0	↑			
L-Galactose	HMDB0033704																			1.33935	0.012	↓			
muco-Inositol	HMDB0062138																						1.54508	0.009	↓

Table 2. List of metabolites that differed significantly in lung, heart, stomach, serum, spleen, intestines, liver and kidney samples from mice after SN-38 treatment.

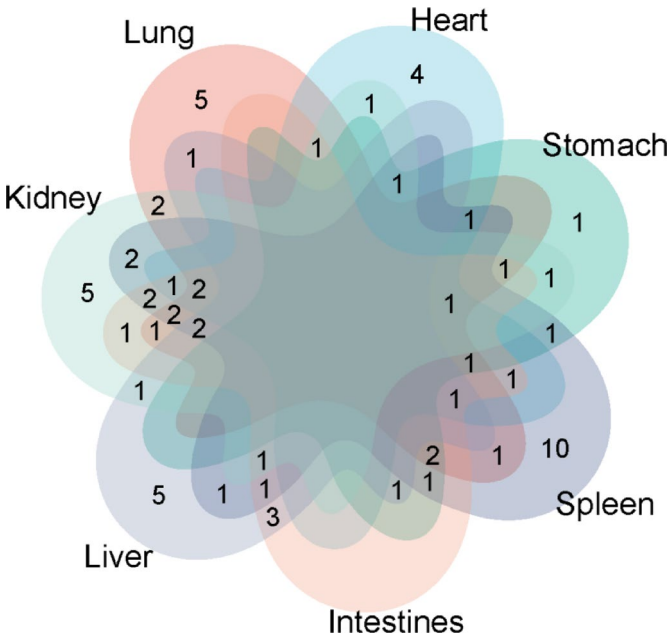

Fig. 3. Venn diagram of the metabolite distribution in the lung, heart, stomach, spleen, intestines, liver, and kidney between the control and SN-38 groups. Note: the numbers in the figure represent the same metabolites among different matrices.

prior to irreversible injury. Conventional histological methods, which detect toxicity only at advanced stages (e.g., necrosis or inflammatory infiltration), lack the sensitivity to identify such subclinical perturbations. In contrast, untargeted GC–MS metabolomics captures subtle metabolic imbalances predictive of incipient organ damage[44]. These findings highlight the predictive potential of metabolomic profiling as a sensitive preclinical screening tool, offering mechanistic insights into subclinical toxicity that precedes histologically detectable lesions.Nonetheless, the absence of physiological and functional validation remains a limitation. Future studies will be directed toward integrating organ-specific functional assays and phenotypic evaluations to confirm the biological consequences of these metabolic changes and further clarify the toxicological profile of SN-38.

Conclusion

A comprehensive analysis of the multi-organ toxicity induced by SN-38 reveals a complex interaction of metabolic disruptions that significantly impair organ function and systemic homeostasis. The lungs, heart, gastrointestinal tract, liver, and blood are the most affected, with purine, pyrimidine, amino acid, and glycerolipid metabolism playing central roles in the toxic effects. These metabolic disturbances suggest impairments in protein synthesis, cellular homeostasis, energy metabolism, and antioxidant defense mechanisms. This integrative metabolomics approach provides critical insights into the mechanisms underlying SN-38 toxicity and highlights potential biomarkers for monitoring and mitigating its adverse effects.

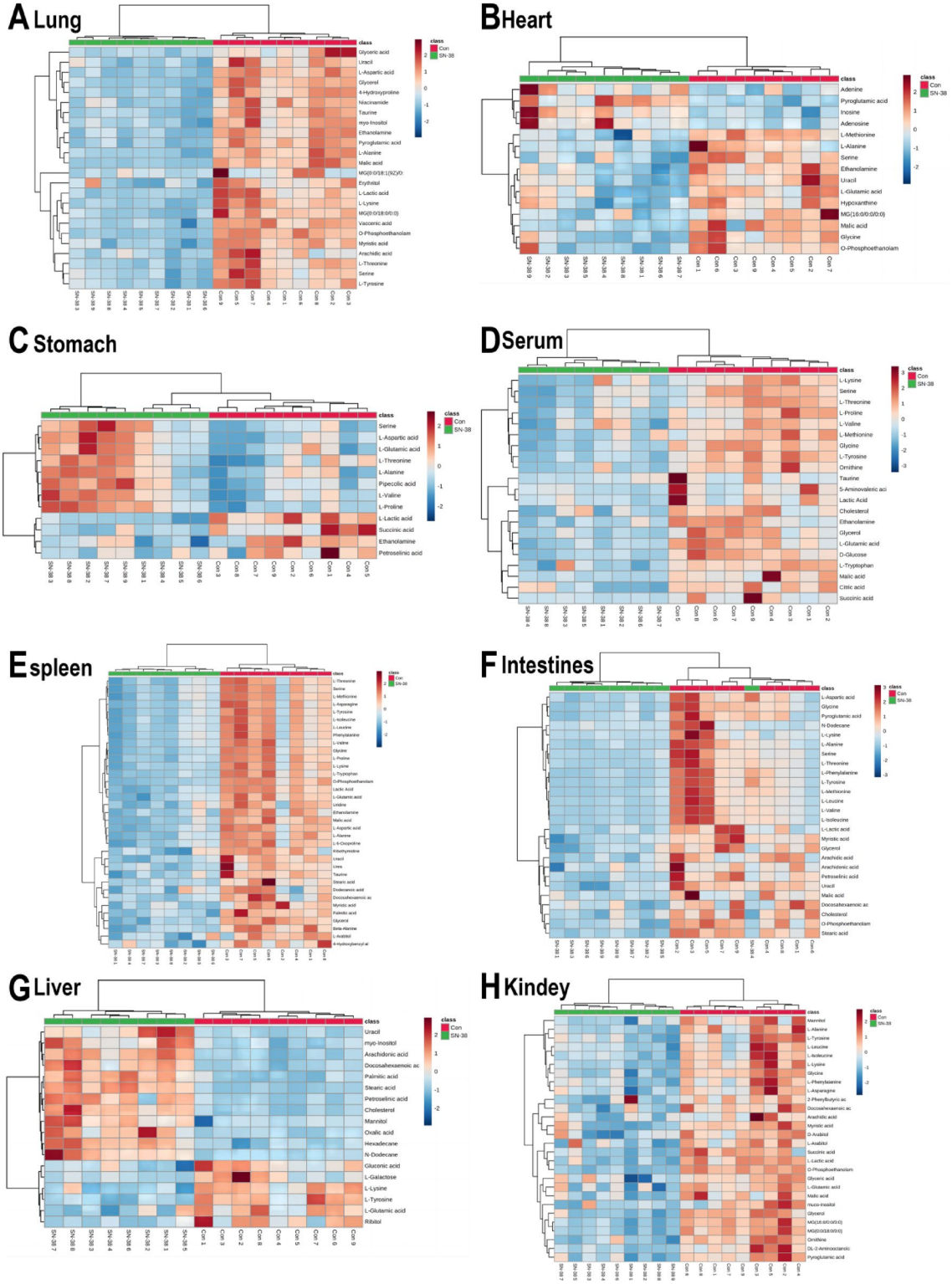

Fig. 4. Heatmap of differential metabolites in the SN-38 group compared to controls. Each color in the heatmap represents metabolite changes: blue indicates down-regulation, and red indicates up-regulation. In the heatmap, columns represent samples and rows represent metabolites.

	Lung			Heart			Stomach			Serum			Spleen			Intestine			Liver			Kidney		
Metabolic Pathway	Raw *p*	FDR	Impact	Raw *p*	FDR	Impact	Raw *p*	FDR	Impact	Raw *p*	FDR	Impact	Raw *p*	FDR	Impact	Raw *p*	FDR	Impact	Raw *p*	FDR	Impact	Raw *p*	FDR	Impact
Glycine, Serine and Threonine Metabolism	0.0088792	0.35053	0.25139	0.037047	0.36597	0.48837	0.023345	0.2312	0.22838	0.0088792	0.11839	0.51302	0.034891	0.27912	0.51302	0.014834	0.16953	0.51302						
Purine Metabolism				0.0030174	0.080463	0.04324																		
Glyoxylate and Dicarboxylate Metabolism	0.0074842	0.35053	0.1217	0.00013756	0.011005	0.14815	0.020803	0.2312	0.04233	3.6323E-5	0.0029058	0.1799	0.004246	0.056614	0.14815	0.012552	0.16736	0.14815				7.4154E-04	0.019774	0.18519
Glutathione Metabolism				0.0017575	0.070299	0.11548				0.0051119	0.08179	0.10839	0.020856	0.18539	0.11548							4.3771E-04	0.017508	0.11548
Alanine, Aspartate and Glutamate Metabolism				0.025758	0.36597	0.19712	2.7399E-05	0.0021919	0.42068	0.0051119	0.08179	0.19712	0.0025701	0.045573	0.42068							4.3771E-04	0.017508	0.19712
Sphingolipid Metabolism				0.033099	0.36597	0.00563																		
Citrate Cycle (TCA Cycle)										0.0019024	0.076095	0.16723										0.029494	0.23595	0.07685
Arginine and Proline Metabolism							0.02601	0.2312	0.01744	0.010418	0.11907	0.18139												
Phenylalanine, Tyrosine and Tryptophan Biosynthesis													0.0026459	0.045573	1	0.0013941	0.052733	1	0.028533	0.80117	0.5	1.0636E-03	0.021271	1
Pyruvate Metabolism	0.034982	0.39979	0.0283							0.034982	0.23321	0.0283				0.049	0.392	0.0283				0.038313	0.27864	0.0283
Glycerophospholipid Metabolism				0.041171	0.36597	0.03747																		
Glycerolipid Metabolism	0.017527	0.35053	0.33022																			0.019254	0.17114	0.33022
Arginine Biosynthesis							0.0040973	0.085769	0.11675	0.013501	0.13501	0.17766	0.0028483	0.045573	0.11675							0.014845	0.16965	0.17766
Primary Bile Acid Biosynthesis										0.02037	0.16296	0.07802												
Beta-Alanine Metabolism													0.0093852	0.10726	0.39925									
Pantothenate and CoA Biosynthesis													6.8742E-04	0.027497	0.04762									
Phenylalanine Metabolism													0.018293	0.18293	0.35714	0.0098689	0.1579	0.35714				0.0075883	0.10118	0.35714
Nicotinate and nicotinamide metabolism	0.015457	0.35053	0.1943																					
Cysteine and methionine metabolism				0.035051	0.36597	0.1263																		
Galactose metabolism										0.04704	0.28948	0.03499												
Pyrimidine metabolism													0.049536	0.30159	0.09246									

Table 3. Metabolic pathways related to SN-38 intervention mechanisms.

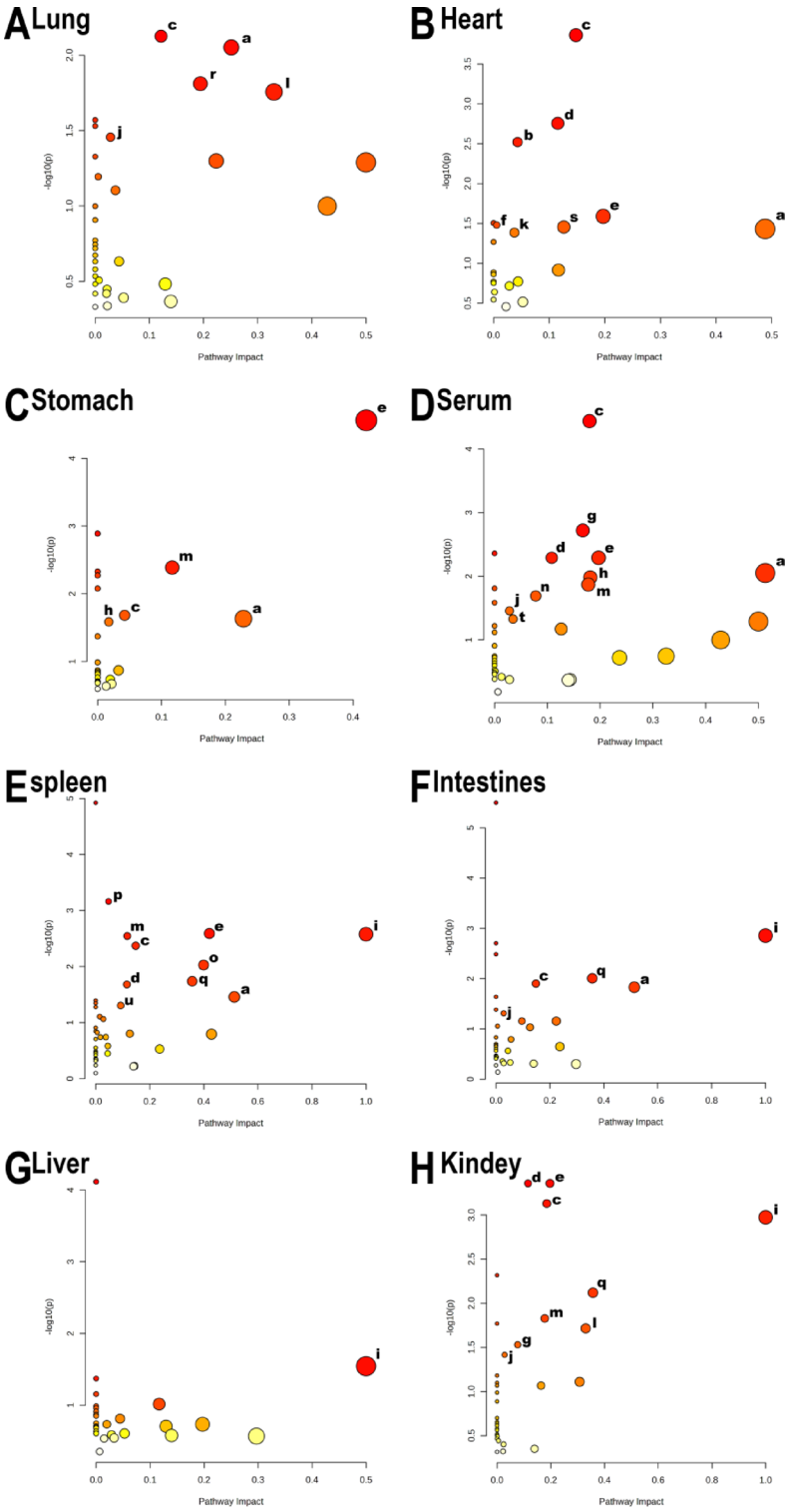

Fig. 5. Summary of the pathway analysis conducted using MetaboAnalyst 6.0:a Glycine, Serine and Threonine Metabolism; b Purine Metabolism; c Glyoxylate and Dicarboxylate Metabolism; d Glutathione Metabolism; e Alanine, Aspartate and Glutamate Metabolism; f Sphingolipid Metabolism; g Citrate Cycle (TCA Cycle); h Arginine and Proline Metabolism; i Phenylalanine, Tyrosine and Tryptophan Biosynthesis; j Pyruvate Metabolism; k Glycerophospholipid Metabolism; l Glycerolipid Metabolism; m Arginine Biosynthesis; n Primary Bile Acid Biosynthesis; o Beta-Alanine Metabolism; p Pantothenate and CoA Biosynthesis; q Phenylalanine Metabolism; r Nicotinate and nicotinamide metabolism; s Cysteine and methionine metabolism; t Galactose metabolism; u Pyrimidine metabolism.

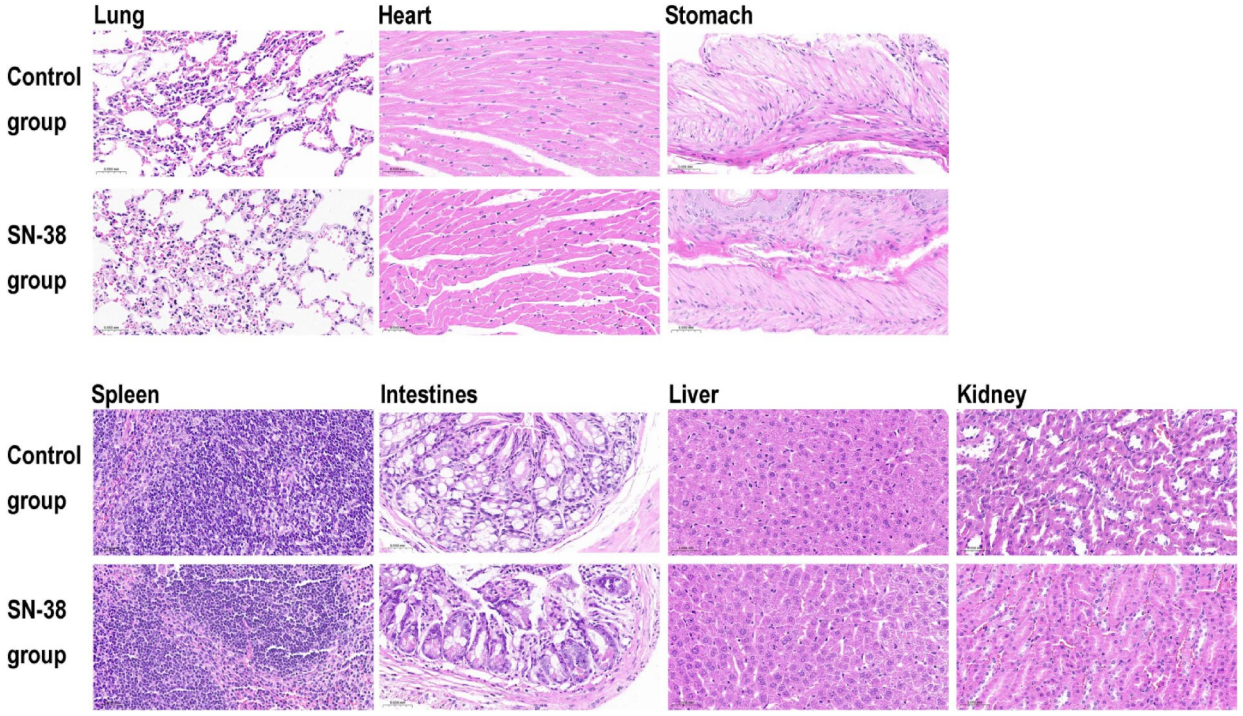

Fig. 6. Tissues stained with hematoxylin and eosin include the lungs, heart, stomach, spleen, intestines, liver and kidney.

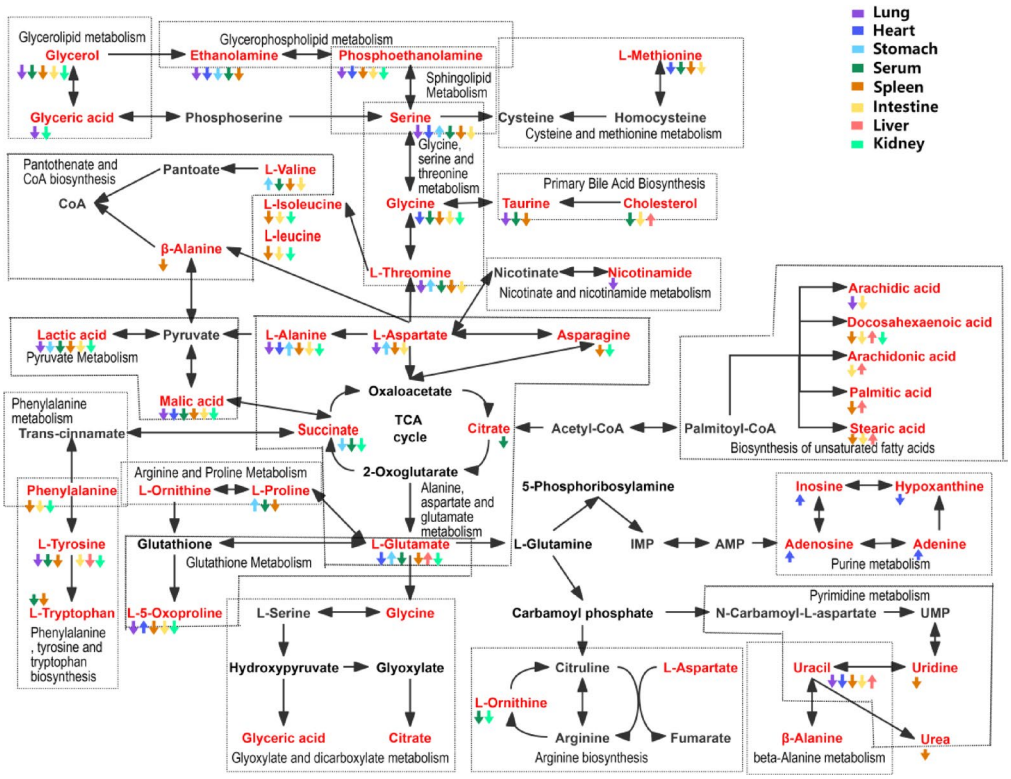

Fig. 7. Schematic diagram illustrating metabolic pathways in tissues affected by SN-38 processing. Metabolites marked in red represent potential biomarkers identified in this study.Directional arrows (▲ for upregulation, ▼ for downregulation) were introduced to unambiguously distinguish metabolite expression trends; A tissue-specific color-coding system was applied to annotate the organ origin of metabolic perturbations.This figure includes data adapted from the KEGG database (© Kanehisa Laboratories). The KEGG pathway map is used with permission from the Kanehisa Laboratory[14–16].

Data availability

The untargeted metabolomics data generated in this study have been deposited in the OMIX repository of the China National Center for Bioinformation (https://ngdc.cncb.ac.cn/omix) under accession number OMIX009615. The dataset will be made publicly available without restriction upon publication of this article. Additional information will be made available upon request (hanguangkui1997@163.com).

Received: 21 December 2024; Accepted: 8 May 2025
Published online: 12 May 2025

References

1. Kciuk, M., Marciniak, B. & Kontek, R. Irinotecan—still an important player in cancer chemotherapy: A comprehensive overview. *IJMS* **21**, 4919 (2020).
2. Han, J., Zhang, J. & Zhang, C. Irinotecan-induced steatohepatitis: current insights. *Front. Oncol.* **11**, 754891 (2021).
3. Xu, S., Lan, H., Huang, C., Ge, X. & Zhu, J. Mechanisms and emerging strategies for irinotecan-induced diarrhea. *Eur. J. Pharmacol.* **974**, 176614 (2024).
4. Yang, J., Jia, L., He, Z. & Wang, Y. Recent advances in SN-38 drug delivery system. *Int. J. Pharm.* **637**, 122886 (2023).
5. Qi, Q., Tian, H., Yue, B., Zhai, B. & Zhao, F. Research progress of SN38 drug delivery system in cancer treatment. *IJN Volume.* **19**, 945–964 (2024).
6. Pang, H., Jia, W. & Hu, Z. Emerging applications of metabolomics in clinical Pharmacology. *Clin. Pharma Ther.* **106**, 544–556 (2019).
7. Shoaib, M. et al. Plasma metabolomics supports the use of long-duration cardiac arrest rodent model to study human disease by demonstrating similar metabolic alterations. *Sci. Rep.* **10**, 19707 (2020).
8. Xiaodong, Z. et al. Investigating the impact of SN-38 on mouse brain metabolism based on metabolomics. *Drug Des. Devel Ther.* **18**, 2435–2447 (2024).
9. Nobre, L. M. S. et al. Paraprobiotic enterococcus faecalis EC-12 prevents the development of irinotecan-induced intestinal mucositis in mice. *Life Sci.* **296**, 120445 (2022).
10. Takeda, M. et al. Disruption of endolysosomal RAB5/7 efficiently eliminates colorectal cancer stem cells. *Cancer Res.* **79**, 1426–1437 (2019).
11. Viant, M. R., Kurland, I. J., Jones, M. R. & Dunn, W. B. How close are we to complete annotation of metabolomes? *Curr. Opin. Chem. Biol.* **36**, 64–69 (2017).
12. Zhiqiang, P. et al. MetaboAnalyst 6.0: towards a unified platform for metabolomics data processing, *Anal. interpretation Nucleic Acids Res.*, **52**, W398–W406 (2024).

13. Zhiqiang, P. et al. MetaboAnalystR 4.0: a unified LC-MS workflow for global metabolomics.Nature Communications volume 15, Article number: 3675 (2024).
14. Kanehisa, M., Furumichi, M., Sato, Y., Matsuura, Y. & Ishiguro-Watanabe, M. KEGG: biological systems database as a model of the real world. *Nucleic Acids Res.* **53**, D672–D677 (2025).
15. Kanehisa, M. Toward Understanding the origin and evolution of cellular organisms. *Protein Sci.* **28**, 1947–1951 (2019).
16. Kanehisa, M. & Goto, S. KEGG: Kyoto encyclopedia of genes and genomes. *Nucleic Acids Res.* **28**, 27–30 (2000).
17. Yun, X. & Royston, G. Mind your Ps and Qs-Caveats in metabolomics data analysis.trends in analytical chemistry volume**183** 118064 (2025).
18. Limper, A. H. Chemotherapy-induced lung disease. *Clin. Chest. Med.* **25**, 53–64 (2004).
19. Ozawa, Y. et al. Preexisting interstitial lung disease and lung injury associated with Irinotecan in patients with neoplasms. *Anticancer Res.* **38**, 5937–5941 (2018).
20. Mir, T. A. et al. Irinotecan inducing sinus pause bradycardia in a patient with small round cell cancer. *BMJ Case Rep.* **13**, e232053 (2020).
21. Agudelo, C. W. & Samaha, G. Garcia-Arcos, I. Alveolar lipids in pulmonary disease. A review. *Lipids Health Dis.* **19**, 122 (2020).
22. Gao, Y. et al. Metabolomic analysis of radiation-induced lung injury in rats: the potential radioprotective role of taurine. *Dose-Response* **17**, 1559325819883479 (2019).
23. He, W. et al. Liang-ge Decoction ameliorates acute lung injury in septic model rats through reducing inflammatory response, oxidative stress, apoptosis, and modulating host metabolism. *Front. Pharmacol.* **13**, 926134 (2022).
24. Nojima, Y. et al. Metabolomic analysis of fibrotic mice combined with public RNA-seq human lung data reveal potential diagnostic biomarker candidates for lung fibrosis. *FEBS Open. Bio.* **10**, 2427–2436 (2020).
25. Guieu, R. et al. Adenosine and the cardiovascular system: the good and the bad. *JCM* **9**, 1366 (2020).
26. Bauer, J. A., Moffatt-Bruce, S. D., Elton, T. S. & Feldman, D. Purine metabolism in heart failure: oxidant biology and therapeutic indications. *Congestive Heart Fail.* **14**, 283–284 (2008).
27. Tan, M. et al. Glutathione system enhancement for cardiac protection: Pharmacological options against oxidative stress and ferroptosis. *Cell. Death Dis.* **14**, 131 (2023).
28. Shosha, M. I., El-Ablack, F. Z. & Saad, E. A. Glycine protects against doxorubicin-induced heart toxicity in mice. *Amino Acids*. **55**, 679–693 (2023).
29. Ciftci, O., Turkmen, N. B. & Taslıdere, A. Curcumin protects heart tissue against irinotecan-induced damage in terms of cytokine level alterations, oxidative stress, and histological damage in rats. *Naunyn-Schmiedeberg's Arch. Pharmacol.* **391**, 783–791 (2018).
30. Xie, D. et al. Systematic metabolic profiling of mice with dextran sulfate sodium-induced colitis. *JIR Volume*. **14**, 2941–2953 (2021).
31. Li, R. et al. CircRNA CDR1as: A novel diagnostic and prognostic biomarker for gastric cancer. *Biomarkers* **28**, 448–457 (2023).
32. Du, J., Li, X. H. & Li, Y. J. Glutamate in peripheral organs: biology and Pharmacology. *Eur. J. Pharmacol.* **784**, 42–48 (2016).
33. Tsai, L. H. Function of GABAergic and glutamatergic neurons in the stomach. *J. Biomed. Sci.* **12**, 255–266 (2005).
34. Yu, Q. Q. et al. Systematic evaluation of irinotecan-induced intestinal mucositis based on metabolomics analysis. *Front. Pharmacol.* **13**, 958882 (2022).
35. Das, U. N. Essential fatty acids and their metabolites in the pathobiology of inflammation and its resolution. *Biomolecules* **11**, 1873 (2021).
36. Wang, W. et al. Ginsenoside Rk3 ameliorates obesity-induced colitis by modulating lipid metabolism in C57BL/6 mice. *J. Agric. Food Chem.* **72**, 2997–3007 (2024).
37. Sonnweber, T., Pizzini, A., Nairz, M., Weiss, G. & Tancevski, I. Arachidonic acid metabolites in cardiovascular and metabolic diseases. *IJMS* **19**, 3285 (2018).
38. Aggarwal, S. et al. Metabolomic analysis shows dysregulation in amino acid and NAD+metabolism in palmitate treated hepatocytes and plasma of non-alcoholic fatty liver disease spectrum. *Biochem. Biophys. Res. Commun.* **643**, 129–138 (2023).
39. Huang, T. et al. Mechanism of the effect of compound anoectochilus Roxburghii (wall.) Lindl. Oral liquid in treating alcoholic rat liver injury by metabolomics. *DDDT Volume*. **17**, 3409–3428 (2023).
40. Glinton, K. E. et al. Disturbed phospholipid metabolism in Serine biosynthesis defects revealed by metabolomic profiling. *Mol. Genet. Metab.* **123**, 309–316 (2018).
41. He, F. et al. L -serine lowers the inflammatory responses during pasteurella multocida infection. *Infect. Immun.* **87**, e00677–e00619 (2019).
42. Yang, L. et al. Serine catabolism feeds NADH when respiration is impaired. *Cell Metabol.* **31**, 809–821e6 (2020).
43. Frascatani, R., Mattogno, A., Iannucci, A., Marafini, I. & Monteleone, G. Reduced taurine serum levels in inflammatory bowel disease. *Nutrients* **16**, 1593 (2024).
44. Fenna, S. & ,Thomas H.,Metabolomics in preclinical drug safety assessment. *Curr. Status Future Trends Metabolites*. **14** (2), 98 (2024).

Author contributions

X.Z., C.C., and G.H. designed and planned the research. X.Z. and Y.H. wrote the main manuscript text. J.L. and B.K. conducted the formal analysis. X.Z., Y.H., and J.L. carried out the investigation. X.Z. handled data curation and prepared all figures. Y.H. was responsible for software implementation. X.Z., C.C., and G.H. contributed to the review and editing of the manuscript. C.C. and G.H. supervised the project and managed its administration. All authors reviewed the manuscript and approved the final submitted version.

Funding

This research was funded by the National Natural Science Foundation of China (Grant No.82302795); Natural Science Foundation of Shandong Province [ZR2023QH094]; Jining Key Research and Development Program [2024YXNS126]; Beijing Huikang Charity Foundation [BHCF20240620].

Declarations

Competing interests

The authors declare no competing interests.

Additional information

Supplementary Information The online version contains supplementary material available at https://doi.org/10.1038/s41598-025-01753-1.

Correspondence and requests for materials should be addressed to G.H.